

Modelling the Point Spread Function of Wide Field Small Aperture Telescopes With Deep Neural Networks – Applications in Point Spread Function Estimation

Peng Jia^{1,4,5*}, Xuebo Wu¹, Zhengyang Li² †, Bo Li², Weihua Wang¹, Qiang Liu¹,

Adam Popowicz³ ‡ and Dongmei Cai¹

¹College of Physics and Optoelectronics, Taiyuan University of Technology, Taiyuan, 030024, China

²Nanjing Institute of Astronomical Optics and Technology CAS, Nanjing, Jiangsu, 210042, China

³Electrical Engineering and Microelectronics, Department of Electronics, Silesian University of Technology, Akademicka 16, 44-100 Gliwice, Poland

⁴Key Laboratory of Advanced Transducers and Intelligent Control Systems, Ministry of Education and Shanxi Province, Taiyuan University of Technology, Taiyuan, 030024, China

⁵Department of Physics, Durham University, DH1 3LE, UK

Accepted XXX. Received YYY; in original form ZZZ

ABSTRACT

The point spread function (PSF) reflects states of a telescope and plays an important role in development of smart data processing methods. However, for wide field small aperture telescopes (WFSATs), estimating PSF in any position of the whole field of view (FoV) is hard, because aberrations induced by the optical system are quite complex and the signal to noise ratio of star images is often too low for PSF estimation. In this paper, we further develop our deep neural network (DNN) based PSF modelling method and show its applications in PSF estimation. During the telescope alignment and testing stage, our method collects system calibration data through modification of optical elements within engineering tolerances (tilting and decentering). Then we use these data to train a DNN. After training, the DNN can estimate PSF in any field of view from several discretely sampled star images. We use both simulated and experimental data to test performance of our method. The results show that our method could successfully reconstruct PSFs of WFSATs of any states and in any positions of the FoV. Its results are significantly more precise than results obtained by the compared classic method - Inverse Distance Weight (IDW) interpolation. Our method provides foundations for developing of smart data processing methods for WFSATs in the future.

Key words: telescopes – methods: numerical – techniques: image processing

1 INTRODUCTION

Telescopes with wide FoV (normally greater than 1°) and small apertures (less than 2 metre) are called WFSATs. They are low-cost, light-weighted and commonly used for wide field sky surveys in time domain astronomy (Burd et al. 2005; Ma et al. 2007; Yuan et al. 2008; Cui et al. 2008; Pablo et al. 2016; Ping & Zhang 2017; Ratzloff et al. 2019; Sun & Yu 2019). Because apertures of WFSATs are small, they are normally used to observe bright targets. To further increase detection and observation abilities of WFSATs, smart data processing methods have been recently developed proving their superiority over existing image processing

techniques (Jia et al. 2020b; Glazier et al. 2020).

Strong prior conditions are necessary for smart data processing methods. These are both the information of observed objects (such as different morphology of different celestial objects) and imaging conditions. The latter mainly include the PSF shape and its variations within the whole FoV. The PSF is the impulse response of an optical system and it reflects states of the whole telescope. For general purpose sky survey telescopes, different smart data processing methods have been recently tested on images with various PSFs and have successfully proved its robustness (González et al. 2018; Duev et al. 2019; Burke et al. 2019; He et al. 2020). However, PSFs of WFSATs are quite different from that of general purpose sky survey telescopes, because WFSATs are often working remotely (lack of maintenance) and images obtained by them have both low sampling rate and fluctuating quality (e.g.

* robinmartin20@gmail.com

† zyli@niaot.ac.cn

‡ adam.popowicz@polsl.pl

due to the high sensitivity of some optical elements to temperature and/or humidity). PSFs of WFSATs have significant deformation in different regions of FoV (Piotrowski & Żarnecki 2010) and they can evolve with time (Jia et al. 2017). It is very hard to design a fully deterministic image processing method that can model spatially and temporally PSFs and other PSF estimation methods are required.

The statistical PSF modelling method is commonly used for WFSATs nowadays. The statistical methods require large amount of star images as samples of PSFs and obtain effective components from these images through either principal component analysis (Jee et al. 2007; Jia et al. 2017; Popowicz 2018; Sun et al. 2020) or denoising autoencoders (Jia et al. 2020c). Because large amount of star images with adequate signal to noise ratio (SNR) are required (Wang et al. 2018), application of such methods is frequently unsuitable for WFSATs that are used for fast sky survey.

The forward PSF modelling method, which was firstly applied in space based telescopes (Krist et al. 2011; Perrin et al. 2012) and later in telescopes with adaptive optics systems (Martin et al. 2016; Fétick et al. 2019; Beltramo-Martin et al. 2019; Fusco et al. 2020), shows good performance in modelling PSFs generated by the atmospheric turbulence with the help of DNN (Jia et al. 2020a). The forward DNN based PSF modelling method (PSF-NET) builds the Monte Carlo model of the imaging process and generates huge number of PSFs to train the DNN. After training, the PSF-NET learns a function that can reflect the response of a telescope (PSF) to a complex system (such as the atmospheric turbulence). For WFSATs, because all lenses and mirrors are manufactured and assembled with predefined tolerances, PSFs of WFSATs can be interpreted as a response of an imaging system to the actual state of optical misalignment together with the actual quality of fabricated optical elements. The distribution of PSFs with different shapes also reflects the impact of external conditions during imaging, like temperature, humidity or wind strength, which can lead to deformation of PSFs. Therefore, we decide to design the PSF estimation technique using current capabilities of artificial intelligence as such algorithms have already proven to be successful in realization of complex tasks in plenty of various fields.

In this paper, we propose the Tel-Net as a novel PSF modelling method for WFSATs. With tolerances of each optical element in WFSATs as prior information, the Tel-Net is trained on various possible realizations of the optical alignment of the telescope. After training, the Tel-Net can output PSFs of WFSATs of any state in any position within the FoV. We introduce the concept and structure of the Tel-Net in Section 2. The performance of the Tel-Net is tested with simulated data in Section 3 and real data in Section 4. We give the conclusions and propose the future work in Section 5.

2 THE TEL-NET

The philosophy of the Tel-Net is quite simple. PSFs in the whole FoV are representations of the telescope state (Li et al. 2015) which can be modelled by a DNN. After we train the Tel-Net with PSFs of a WFSAT in different states, the Tel-Net will be able to output all PSFs within the whole FoV with only some PSFs given at its input. Therefore, the structure of the DNN in Tel-Net and the way to obtain PSFs as training dataset are two important factors for the

Tel-Net model.

The structure of the DNN in Tel-Net is adopted from the PSF-NET proposed in Jia et al. (2020a) and the DAE-NET proposed in Jia et al. (2020c). The structure of the Tel-Net is shown in figure 1, which has an encoding and decoding structure with DNN blocks to increase its representation ability. Besides we introduce the fixed-update initialization (also known as Fixup method proposed by Zhang et al. (2019)) in the Tel-Net. The Fixup method is a regularization method that rescales weights of all layers in DNNs properly at the beginning of training. Comparing with other ordinary regularization methods, such as the normalization layers (Ba et al. 2016), the Fixup method can accelerate convergence and improve generalization without changing greyscale values of input images. Introduction of the Fixup method would benefit in applications of astronomical image processing, because in astronomical images the grey values have a wider range than that in typical 8-bit images. With the Fixup method, we design several Fixup blocks as DNN blocks to increase the representation ability of the Tel-Net.

There are two possible ways to obtain PSFs to train the Tel-Net: computation-based PSFs or data-driven PSFs. We can obtain PSFs of any position in the whole FoV for a WFSAT in any states through physical computation (Jia et al. 2020a). However, because there are differences between physical computation based PSFs and PSFs in real observed images, the former can only be used as pre-trained data. PSFs that are obtained from real observations (data-driven PSFs) are required for real applications. Due to hardware limitations or the time consumptions in obtaining PSFs in any position of the FoV during real observation, data-driven PSFs can only be obtained for a WFSAT with finite states in several predefined positions in the FoV and with finite accuracy. Due to the low spatial sampling rate in WFSATs images, there would be pixel or sub-pixel level position uncertainties for data-driven PSFs. These problems will be further discussed in Section 3 and Section 4. In this paper, we use data-driven PSFs to train the Tel-Net.

In Tel-Net, PSFs of WFSATs in one state are represented by a data cube (PSF-Cube) with dimensions of $N \times N \times M$, where N stands for width and length of star images and M stands for the number of PSFs that are used to represent a given FoV. In this paper, we divide the FoV of WFSATs into M small sections with equal size (called patches) and we assume that PSFs are uniform in each patch (La Camera et al. 2015). These PSFs are arranged from left to right and top to bottom according to positions of patches in the FoV. Each PSF in a PSF-Cube is aligned with its brightest pixel in the centre. Besides, to reduce effects brought by sub-pixel uncertainties and to extend the training set, we randomly shift PSFs by a fraction of a pixel (from -0.5 to 0.5 with uniform probability distribution) when we obtain PSF-Cubes.

The input and output of the Tel-Net are both PSF-Cubes of the same size. In input PSF-Cubes, only limited PSFs are valid PSFs and the rest of them are zero matrices. In output PSF-Cubes, all PSFs are valid PSFs. Because the Tel-Net should be able to predict all PSFs from several known PSFs, the input and output PSF-Cubes that correspond to the same state of the WFSAT are used as a pair of training data for the Tel-Net. During the training stage, the batch size is set to 4 and we choose the Adam Optimizer (Kingma & Ba 2014) as the optimization algorithm. The learning rate is set as 0.01 and the loss function is L_1 norm defined in equation 1, where n equals to the batch size, $TelNet(PSFCube_{in})$ is the output PSF-

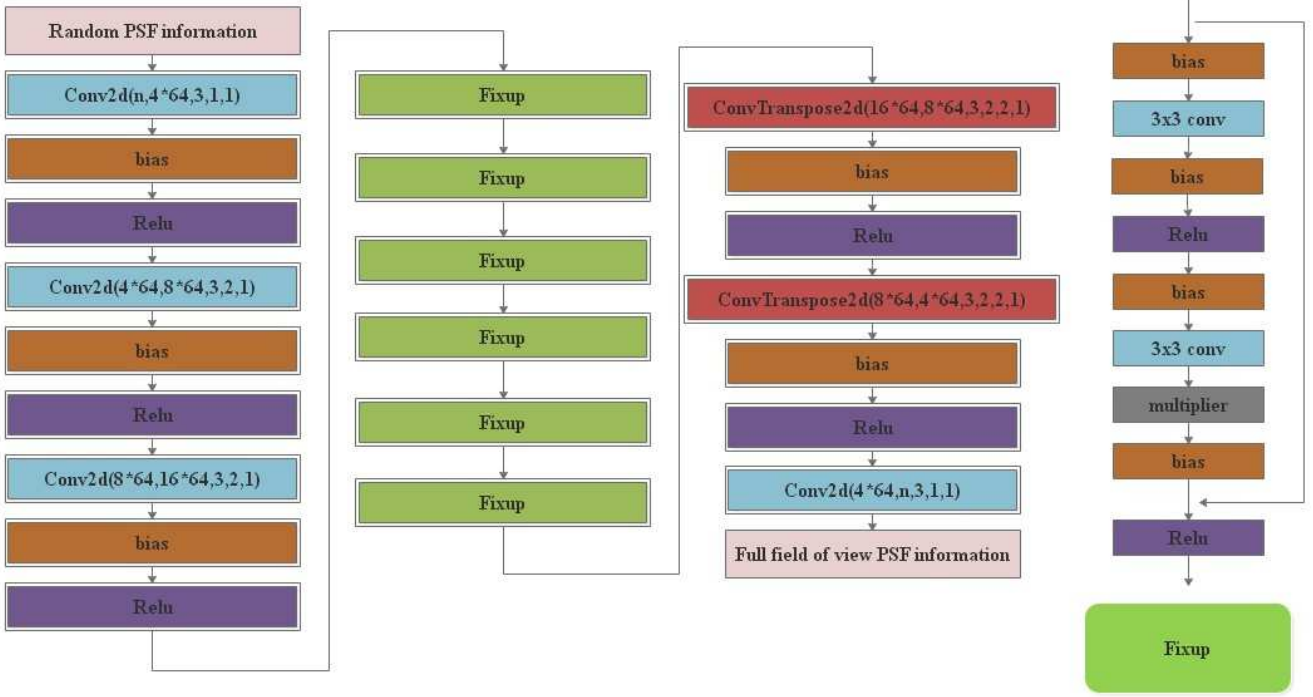


Figure 1. The structure of the Tel-Net. The Tel-Net consists of convolutional layers (Conv2d in blue), Bias layers (Bias in brown), Activation layers (Relu in purple), Conv-transpose layers (ConvTranspose2d in red), multiply layers (multiplier in grey) and Fixup blocks (Fixup block in green). The structure of Fixup block is shown in the right part of this figure.

Cube obtained from the Tel-Net and the $PSFCube_{out}$ is expected output PSF-Cube, the norm $\|$ utilizes the absolute difference.

$$L = \frac{1}{n} \sum_{k=1}^n |TelNet(PSFCube_{in}) - PSFCube_{out}| \quad (1)$$

3 TRAINING AND TESTING OF THE TEL-NET WITH SIMULATED DATA

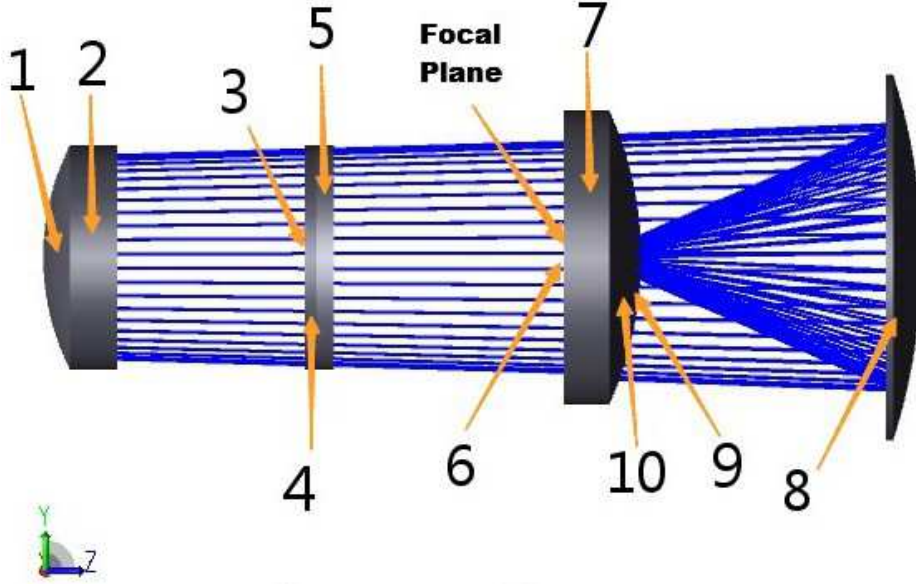
In this section, we simulate a classic WFSAT (Baker super-Schmidt telescope) with ZEMAX to test the performance of the Tel-Net. Parameters of this WFSAT is shown in figure 2. This WFSAT has a field of view of 10° and we divide its field of view equally into 61×61 patches. In each patch, variations of PSFs are small thus a single PSF is representative. There are four optical elements in this telescope and we assume that the second lens has alignment error. There are six free dimensions for the second lens: decenter and tilt along x, y and z directions. To make sure that star images in different places within the FoV can be obtained by the WFSAT, we set the tolerance of the second lens as: -3 millimetres to 3 millimetres with step of 1.5 millimetres for x, y and z decenter, -0.2 degree to 0.2 degree with step of 0.1 degree for x and y tilt. In total, there are 2000 different states for this element and we could obtain 2000 PSF-Cubes. In each PSF-Cube, there are 61×61 PSFs and we obtain 744200 PSFs in total for the training set of the Tel-Net. Meanwhile, we generate 100 PSF-Cubes with the same WFSAT and this time we set the second mirror in random states within its misalignment configurations as the test set.

It should be noted that in essence PSF-Cubes in the training set are sparse samples of all PSFs that correspond to the WFSAT within tolerances of its secondary mirror. Because we sampled

tolerances with relatively big steps, there are still large number of PSFs that can be obtained. Assuming all elements have the same number of free states as the second element, there would be tens of thousands of PSF-Cubes to be obtained, which is impossible for real applications. However, for PSF estimation tasks, many of these states overlap each other: although the telescope belongs to two different states, PSFs in a given point within FoV are almost the same. This is why we decided to make a trade-off between complexity and accuracy. So we use sparsely sampled PSF-Cubes to train the Tel-Net. In the future, we are going to further investigate possible methods of the optimal reduction (minimization) of the training set to its most informative subset.

First of all, we test the robustness of the Tel-Net using a small data set, which includes only 200 PSF-Cubes reflecting states of the WFSAT along tilt of x and y and decenter of x. We select 150 from 200 PSF-Cubes to train the Tel-Net. For the input PSF-Cubes, we randomly select 60 PSFs as known PSFs and set all other PSFs to zero matrices. For the output PSF-Cubes, we use the same PSF-Cube with all PSFs as valid PSFs. After training, we select the remaining 50 PSF-Cubes to test the Tel-Net.

Meanwhile we use direct interpolation method for comparison. We select the Inverse Distance Weight (IDW) interpolation method (Lu & Wong 2008) as classic interpolation method. The IDW interpolation method is a commonly used weighted average interpolation method in which the weights depend on the reciprocal of the distance between interpolated points. We use the mean square error between predicted PSFs and original PSFs as the evaluation function. The statical results of the MSE are shown in table 1 and histograms of the MSE are exposed in figure 3. We can find that with only a limited number of PSFs, the Tel-Net could



Surface	Surface Type	Radius (mm)	Separation (mm)	Glass	Semi-Diameter (mm)
1	Spherical	225.0	42.8	BK7	164.5
2	Spherical	191.3	197.5	Air	143.8
3	Even Aspherical (0, -5.6×10^{-10} , -2.4×10^{-14})	Infinity	14.0	F2	98.6
4	Spherical	-1355.0	13.0	SK2	101.1
5	Plane	Infinity	239.2	Air	105.1
6	Spherical	-293.1	42.8	BK7	177.5
7	Spherical	-324.2	251.0	Air	196.3
8	Spherical	-550.0	-251.0	Mirror	290.8
9	Spherical	-324.2	-42.8	BK7	119.9
10	Spherical	-293.1	-14.5	Air	95.1
Focal Plane	Spherical	-241.8	-	-	82.6

Figure 2. Parameters of a simulated WFSAT with Baker super-Schmidt design. The third surface is an even aspherical surface and the aspherical coefficients are also shown in this table

Table 1. MSE between predicted PSFs (estimated by the Tel-Net and the IDW) and original PSFs. The Tel-Net is trained by 150 training PSF-Cubes and tested by other 50 test PSF-Cubes.

Predicted Method	MSE mean	MSE variance
Tel-Net	3.77×10^{-8}	2.76×10^{-16}
IDW	8.01×10^{-7}	2.09×10^{-13}

still be able to predict PSFs with relatively high accuracy, while the existing IDW method presents a magnitude higher MSE. An example of original PSF, a Tel-Net predicted PSF and an IDW predicted PSF are shown in figure 4. We can find that:

1. PSFs of WFSATs have irregular shape;
2. PSFs obtained by the interpolation method can not retain complex shapes, which is probably the reason why our method has much better predictions than the IDW method;
3. Tel-Net has both low mean MSE and low variance of MSE which indicates high repeatability good results of this estimator.

In the next step, we test the performance of the Tel-Net with a bigger dataset. This time we use the entire 2000 PSFs that are defined in the beginning of this section. We use 100 PSF-Cubes with random misalignments of the secondary mirror as the test set. The Tel-Net is trained through 10 epochs which is enough to achieve reasonable abilities. The statistical results of the MSE are

Table 2. MSE between predicted PSFs (estimated by the Tel-Net and the IDW) and original PSFs. The Tel-Net is trained by 2000 training PSF-Cubes and tested by 100 test PSF-Cubes.

Predicted Method	MSE mean	MSE variance
Tel-Net	1.49×10^{-8}	5.81×10^{-17}
IDW	7.79×10^{-7}	2.04×10^{-13}

shown in table 2 and the histograms of the MSE are shown in figure 5. The results show that the Tel-Net has better ability to model PSFs in fine details than the interpolation method. The residual error is almost one order smaller than the interpolation method. It indicates us that with adequate sampled PSFs as training set, the Tel-Net could almost predict any PSFs of WFSATs in any states.

4 TRAINING AND TESTING TEL-NET WITH EXPERIMENTAL DATA

To further test the performance of the Tel-Net, we set up an optical experimental bench in the laboratory according to the schema given in figure 6 and with the experiment setup presented in figure 7. It includes a parabolic mirror (M3), an Ritcher-Chretien (RC) telescope with wavefront error (RMS value) less than $1/30\lambda$ (M1 and M2), a fibre laser as a point-like source of light and a camera

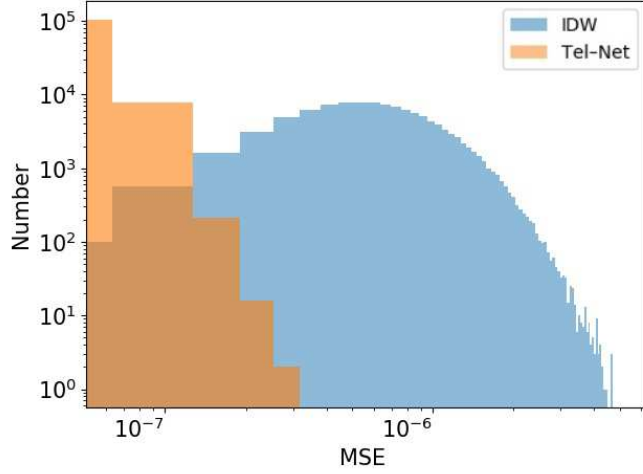


Figure 3. Brown is histogram of MSE between PSFs predicted by Tel-Net and original PSFs, blue is the histogram of MSE between PSFs predicted by IDW and original PSFs. The Tel-Net is trained by 150 training PSF-Cubes and tested by the other 50 test PSF-Cubes.

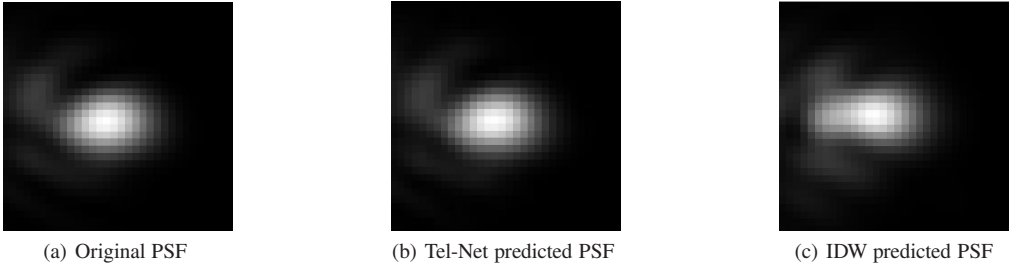


Figure 4. (a) is the original PSF, (b) is PSF predicted by the Tel-Net and (c) is PSF predicted by the IDW with with four nearby PSFs used for interpolation.

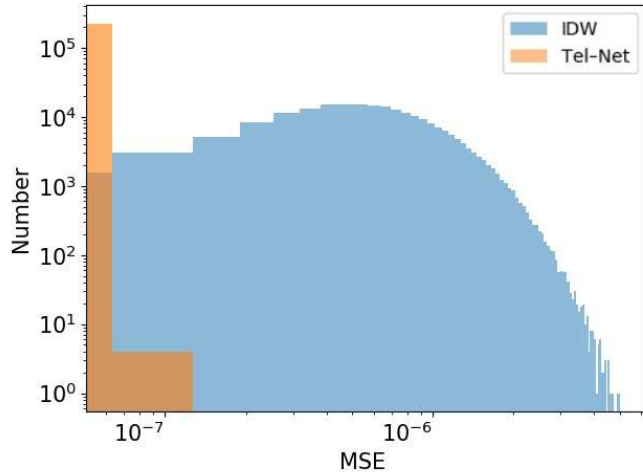


Figure 5. Brown is histogram of MSE between PSFs predicted by Tel-Net and original PSFs, blue is the histogram of MSE between PSFs predicted by IDW and original PSFs. The Tel-Net is trained by 2000 training PSF-Cubes and tested by 100 test PSF-Cubes.

(CCD). We tilt the parabolic mirror (M3) to introduce additional aberrations and then move the camera together with the telescope to obtain PSFs in different positions in FoV. In total we generate 40 different levels of M3 tilts. For each levels of tilt, we obtain 25 PSFs equally distributed in 5×5 patches. An exemplary PSF

obtained at the edge of the FoV is shown in figure 8.

Because automatic alignment devices such as electric precise lifting platforms are not used in this experiment, tilt of M3 and capture of PSFs are all done manually. Therefore, although we have spent a long time to collect PSFs, only very

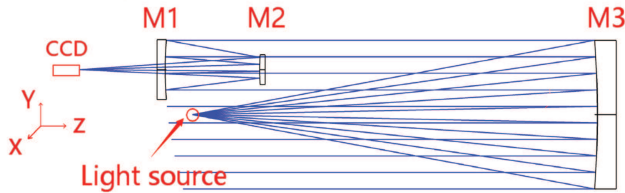


Figure 6. The concept design of the optical path in our experiment.

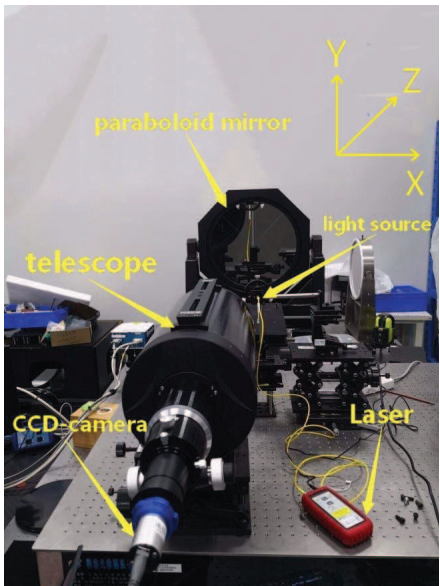


Figure 7. The optical path utilized in our experiment.

limited data are obtained, comparing with the amount of data generated previously by ZEMAX. Besides due to limitations of human beings, these data have obvious imperfections: different levels of tilts are not strictly equally distributed and PSFs of the same patch corresponding to different tilts have position uncertainties up to several pixels. These problems impose the need for the use of automatic alignment instruments and related control methods while calibrating the smart data processing algorithms.

Although these PSFs have some issues, we still try to train the Tel-Net with these data to test its robustness. In total, we obtain 40 PSF-Cubes and we randomly select 36 PSF-Cubes to train the Tel-Net. 8 PSFs are randomly selected as known PSFs in input PSF-Cubes. After training, we use the Tel-Net to predict PSFs with PSF-Cubes from the test set. One of PSFs predicted by the Tel-Net and that predicted by the IDW method are shown in figure 8. The Tel-Net can predict PSFs in fine details, while the IDW method can only predict main structure of the original PSF. Histogram and statistical results of reconstruction error are shown in figure 9 and table 3. We can find that the Tel-Net has better performance than that of the IDW method, even with very limited data.

5 CONCLUSIONS AND FUTURE WORK

In this paper, we propose the Tel-Net as a new PSF modelling framework for WFSATs. The Tel-Net assumes that PSFs in

Table 3. MSE between predicted PSFs (estimated by the Tel-Net and the IDW) and original PSFs. The Tel-Net is trained by 36 training PSF-Cubes and tested by 4 PSF-Cubes.

Type	mean	var
Tel-Net	1.29×10^{-6}	3.07×10^{-12}
IDW	2.83×10^{-6}	5.60×10^{-12}

WFSATs can be understood as a response of a complex system for a single state of an imaging instrument. States of the whole optical system are sampled by PSF-Cubes during system test procedure. Then we train the Tel-Net with PSF-Cubes and use it to predict PSFs. We test the Tel-Net with simulated and real data and find that the Tel-Net can obtain PSFs in any positions of the FoV with finite star images. An example of classic PSF estimation method, the interpolation method utilizing the Inverse Distance Weighting has significantly worse performance and is not able to predict complex aberrations seen in both real and simulated PSFs.

The Tel-Net could be used as a standard calibration method for WFSATs, particularly for WFSATs that are lack of maintenance during observations, such as space telescopes. The Tel-Net indicates the importance of test data of a WFSAT pointing out the need for automatic characterization of the optical instrument during commissioning phase. In the future, we will apply the Tel-Net for a WFSAT and solve the problem of proper reduction of the training set without loosing the high performance of the net.

ACKNOWLEDGEMENTS

Peng Jia would like to thank Dr. Alastair Basden from Durham University, Professor Rongyu Sun from Purple Mountain Observatory who provide very helpful suggestions for this paper. This work is supported by National Natural Science Foundation of China (NSFC)(11503018), the Joint Research Fund in Astronomy (U1631133) under cooperative agreement between the NSFC and Chinese Academy of Sciences (CAS). Authors acknowledge the French National Research Agency (ANR) to support this work through the ANR APPLY (grant ANR-19-CE31-0011) coordinated by B. Neichel. This work is also supported by Shanxi Province Science Foundation for Youths (201901D211081), Research and Development Program of Shanxi (201903D121161), Research Project Supported by Shanxi Scholarship Council of China, the Scientific and Technological Innovation Programs of Higher Education Institutions in Shanxi (2019L0225).

Data Availability Statements: the code in this paper can be downloaded from aojp.lamost.org and after acceptance the code will be released in PaperData Repository powered by China-VO with a DOI number.

REFERENCES

Ba J. L., Kiros J. R., Hinton G. E., 2016, arXiv preprint arXiv:1607.06450
 Beltramo-Martin O., Correia C., Ragland S., Jolissaint L., Neichel B., Fusco T., Wizinowich P., 2019, Monthly Notices of the Royal Astronomical Society, 487, 5450
 Burd A., et al., 2005, in Photonics Applications in Industry and Research IV. p. 59481H
 Burke C. J., Aleo P. D., Chen Y.-C., Liu X., Peterson J. R., Sembroski G. H., Lin J. Y.-Y., 2019, *MNRAS*, 490, 3952

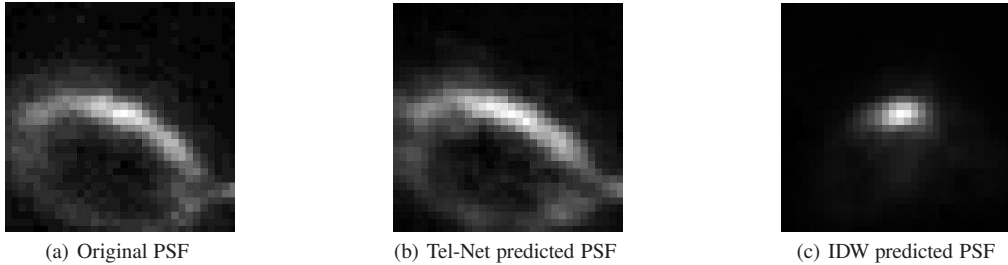


Figure 8. (a) is the original PSF, (b) is PSF predicted by the Tel-Net and (c) is PSF predicted by the IDW with four PSFs as prior information.

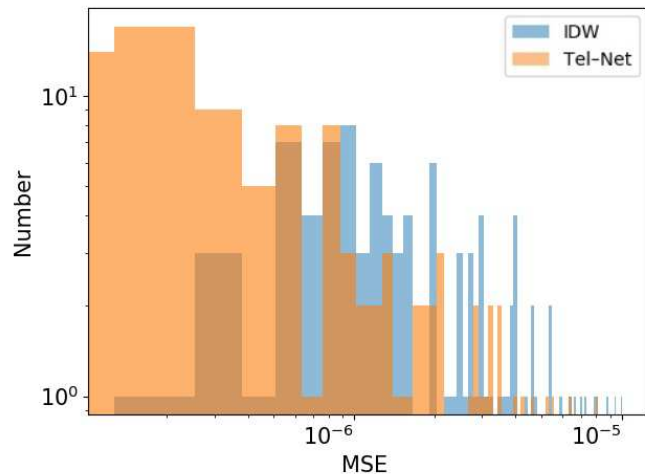


Figure 9. Brown is the MSE histogram of the Tel-Net between estimated PSFs and original PSFs, blue is the MSE histogram of the IDW method between estimated PSFs and original PSFs.

Cui X., Yuan X., Gong X., 2008, in *Ground-based and Airborne Telescopes II*. p. 70122D

Duev D. A., et al., 2019, *MNRAS*, **486**, 4158

Fétick R., et al., 2019, *Astronomy & Astrophysics*, **628**, A99

Fusco T., et al., 2020, *Astronomy & Astrophysics*, **635**, A208

Glazier A. L., Howard W. S., Corbett H., Law N. M., Ratzloff J. K., Fors O., del Ser D., 2020, arXiv e-prints, [p. arXiv:2006.14712](https://arxiv.org/abs/2006.14712)

González R. E., Muñoz R. P., Hernández C. A., 2018, *Astronomy and Computing*, **25**, 103

He Z., et al., 2020, *MNRAS*,

Jee M. J., Blakeslee J. P., Sirianni M., Martel A. R., White R. L., Ford H. C., 2007, *PASP*, **119**, 1403

Jia P., Sun R., Wang W., Cai D., Liu H., 2017, *MNRAS*, **470**, 1950

Jia P., Wu X., Yi H., Cai B., Cai D., 2020a, *AJ*, **159**, 183

Jia P., Liu Q., Sun Y., 2020b, *AJ*, **159**, 212

Jia P., Li X., Li Z., Wang W., Cai D., 2020c, *MNRAS*, **493**, 651

Kingma D. P., Ba J., 2014, arXiv preprint arXiv:1412.6980

Krist J. E., Hook R. N., Stoehr F., 2011, in *Proc. SPIE*. p. 81270J, [doi:10.1117/12.892762](https://doi.org/10.1117/12.892762)

La Camera A., Schreiber L., Diolaiti E., Boccacci P., Bertero M., Bellazzini M., Ciliegi P., 2015, *Astronomy & Astrophysics*, **579**, A1

Li Z., Yuan X., Cui X., 2015, *Monthly Notices of the Royal Astronomical Society*, **449**, 425

Lu G. Y., Wong D. W., 2008, *Computers & geosciences*, **34**, 1044

Ma Y., Zhao H., Yao D., 2007, in Valsecchi G. B., Vokrouhlický D., Milani A., eds, *IAU Symposium Vol. 236, Near Earth Objects, our Celestial Neighbors: Opportunity and Risk*. pp 381–384, [doi:10.1017/S1743921307003468](https://doi.org/10.1017/S1743921307003468)

Martin O., et al., 2016, in *Adaptive Optics Systems V*. p. 99091Q

Pablo H., et al., 2016, *PASP*, **128**, 125001

Perrin M. D., Soummer R., Elliott E. M., Lallo M. D., Sivararamakrishnan A., 2012, in *Proc. SPIE*. p. 84423D, [doi:10.1117/12.925230](https://doi.org/10.1117/12.925230)

Ping Y., Zhang C., 2017, *Advances in Space Research*, **60**, 907

Piotrowski L. W., Żarnecki A. F., 2010, in Leroy C., Rancoita P.-G., Barone M., Gaddi A., Price L., Ruchti R., eds, *Astroparticle, Particle and Space Physics, Detectors and Medical Physics Applications*. pp 313–318, [doi:10.1142/9789814307529_0051](https://doi.org/10.1142/9789814307529_0051)

Popowicz A., 2018, in *Proc. SPIE*. p. 1069820, [doi:10.1117/12.2299498](https://doi.org/10.1117/12.2299498)

Ratzloff J. K., Law N. M., Fors O., Corbett H. T., Howard W. S., Ser D. D., Haislip J. B., 2019, *Publications of the Astronomical Society of the Pacific*, **131**, 075001

Sun R., Yu S., 2019, *Astrophysics and Space Science*, **364**, 39

Sun R., Yu S., Jia P., Zhao C., 2020, *Monthly Notices of the Royal Astronomical Society*, **497**, 4000

Wang W., Jia P., Cai D., Liu H., 2018, *MNRAS*, **478**, 5671

Yuan X., et al., 2008, in *Ground-based and Airborne Telescopes II*. p. 70124G

Zhang H., Dauphin Y. N., Ma T., 2019, arXiv preprint arXiv:1901.09321

This paper has been typeset from a *TeX/LaTeX* file prepared by the author.